Impact of pressure, salt concentration and temperature on the convective dissolution of carbon dioxide in aqueous solutions

V. Loodts,[1, a)] L. Rongy,[1] and A. De Wit[1]

Nonlinear Physical Chemistry Unit, Faculté des Sciences, Université libre de Bruxelles (ULB), CP231, 1050 Brussels, Belgium.

The convective dissolution of carbon dioxide (CO_2) in salted water is theoretically studied to determine how parameters such as CO_2 pressure, salt concentration and temperature impact the short-time characteristics of the buoyancy-driven instability. On the basis of a parameter-free dimensionless model, we perform a linear stability analysis of the time-dependent concentration profiles of CO_2 diffusing into the aqueous solution. We explicit the procedure to transform the predicted dimensionless growth rate and wavelength of the convective pattern into dimensional ones for typical laboratory-scale experiments in conditions close to room temperature and atmospheric pressure. This allows to investigate the implicit influence of the experimental parameters on the characteristic length and time scales of the instability. We predict that increasing CO_2 pressure, or decreasing salt concentration or temperature destabilizes the system, leading to a faster dissolution of CO_2 into salted water.

PACS numbers: 47.20.Bp, 47.56.+r

[a)] Electronic mail: vloodts@ulb.ac.be

When carbon dioxide (CO_2) dissolves in an aqueous solution, a buoyancy-driven fingering instability can develop because of the formation of a denser layer of CO_2-rich solution on top of the less dense water. By a theoretical analysis, we predict how the short-time characteristics of this instability depend on experimental control parameters. To do so, we use a linear stability analysis based on a parameter-free model along with empirical correlations to compute the characteristic time and length scales of the fingering instability. We find that the growth rate of the convective instability increases with increasing CO_2 pressure or decreasing salt concentration or temperature. These results allow to interpret experimental data[1,2] on the impact of salt concentration and gaseous CO_2 pressure on the convective dissolution of CO_2. Another main result of our analysis is that temperature has only a slight effect for CO_2 pressures close to atmospheric pressure. This study therefore suggests that carefully controlling the temperature of the setup is not needed for reproducibility of experimental studies of convective dissolution of CO_2 in laboratory conditions.

I. INTRODUCTION

The convective mixing of CO_2 with aqueous solutions is a key process for the sequestration of CO_2 in saline aquifers. CO_2 sequestration is one of the several techniques considered to reduce the emissions of CO_2 to the atmosphere, with a view to mitigating climate change[3]. Among possible geological sites for CO_2 sequestration, saline aquifers are promising candidates because, unlike hydrocarbon reservoirs, they are evenly distributed in various parts of the world[3,4]. Upon injection in a saline aquifer, the less dense CO_2 rises above the aqueous phase and spreads laterally under the upper impermeable cap rock. As CO_2 dissolves into the salted water, the resulting CO_2-rich solution is denser than the salted water located below it in the gravity field. The contact zone between these two solutions becomes unstable and develops buoyancy-driven fingering. The resulting convective mixing[5] accelerates the dissolution of CO_2 as it is transported faster further away from the interface, thus speeding up the storage process in underground aquifers and favoring further dissolution. To assess the efficiency of such a convective dissolution process, there is a need to quantify how this

buoyancy-driven instability affects the dynamics of CO_2 sequestration.

As *in-situ* measurements in sequestration sites are difficult to do, laboratory-scale experiments are needed to benchmark the theoretical modeling of the convective dissolution of CO_2 into aqueous solutions. These experiments are typically carried out in vertical Hele-Shaw cells, which consist of two transparent plates separated by a small gap (≤ 1 mm). For small enough gap widths, the flow evolution in a Hele-Shaw cell is described by Darcy's equations similar to the evolution equations for flows in porous media[5]. Hence, such reactors can be used as a simplified experimental analogue of a porous medium with easy visualization of flow dynamics, by using for example a pH-sensitive indicator[1,6,7], a dye[8], a colored solute[9], Mach-Zender interferometry[10], shadowgraphy[11], or Schlieren techniques[12].

Among these laboratory-scale experiments, some of them have been conducted using analogues of CO_2 dissolving into water, like for instance two miscible fluids[8,11] or a solid dissolving into water[9]. The other studies have used gaseous CO_2 dissolving in aqueous solutions dyed by a pH indicator at conditions close to room temperature and atmospheric pressure[1,6,7]. Kneafsey and Pruess[6,7] quantified the transfer of gaseous CO_2 down to water contained in a Hele-Shaw cell with or without beads by measuring the area of the pH-depressed zone and the decrease in CO_2 pressure. They also measured the average wavelength of the fingers as a function of time. In a similar set-up, Outeda *et al.*[1] computed experimental dispersion curves in the early stages of the instability. They evaluated the growth rate and wavenumber of the most unstable convection mode as a function of the pressure of CO_2 and of the concentration of the pH-sensitive indicator. Using a glass tube, Farajzadeh *et al.*[2] studied how the mass transfer of CO_2 into aqueous solutions containing a salt and/or a surfactant is enhanced by increasing the pressure in the gas phase.

Quantitative comparison of these experimental results with theoretical predictions remains however difficult as current theoretical works do not explicitly consider the influence of experimental control parameters on the characteristics of the instability. Such parameters are, for instance, CO_2 pressure, salt concentration and temperature, which can easily be tuned in laboratory-scale experiments. The influence of pressure on CO_2 convective dissolution has been studied experimentally by Outeda *et al.*[1] and Farajzadeh *et al.*[2]. Both works show that increasing CO_2 pressure enhances convection but, to the best of our knowledge, no theoretical work has been performed to explain these trends. Similarly, studying the influence of salt concentration on the buoyancy-driven instability has not been done

yet, despite its relevance for sequestration as possible storage sites for CO_2 often contain variable quantities of dissolved salts. The influence of temperature on the characteristics of the instability has not been investigated either, although it could impact laboratory-scale experiments on CO_2 convective dissolution as experiments are typically carried out without any control of the temperature. There is therefore a need to test whether the properties of the instability are sensitive to changes of temperature by a few degrees, in which case, it might be necessary to maintain the temperature constant, for example by placing the Hele-Shaw cell in a thermostat, to ensure the reproducibility of the measurements[13].

In this context, we study theoretically the influence of these three experimental control parameters (pressure of the gas, salt concentration in the aqueous phase and temperature) on the buoyancy-driven instability that develops during the dissolution of CO_2 in salted water. We use a one-phase model of convective dissolution focusing on the dynamics in the aqueous phase, and perform a linear stability analysis (LSA). We discuss the implicit influence of the experimental parameters on the time and length scales needed to switch from dimensionless theoretical results to dimensional predictions, and therefore explicit their influence on the stability properties of the system.

The outline of the article is the following: in section II, we present the theoretical model and nondimensionalize the equations. In section III, we compute the diffusive base state profile of the CO_2 concentration dissolved in salted water and describe the linear stability analysis used to determine the influence of experimental parameters on the stability of the system. We present our dimensionless results and the way to compute the scalings in section IV. Finally, we study the influence of experimental parameters on the dimensional characteristics of the instability in section V and conclude with a discussion and some prospects for further research in section VI.

II. MODEL

We consider a two-dimensional porous medium or Hele-Shaw cell vertically oriented in the gravity field. At time $\tilde{t} = 0$, gaseous CO_2 is placed above an aqueous solution containing a salt in concentration B_0 along a fixed horizontal flat interface (see figure 1). Gaseous CO_2 dissolves across the interface and diffuses down in the salted water. Although in the context of CO_2 dissolution into oil, Rongy, Haugen, and Firoozabadi[14] modeled the CO_2 gaseous

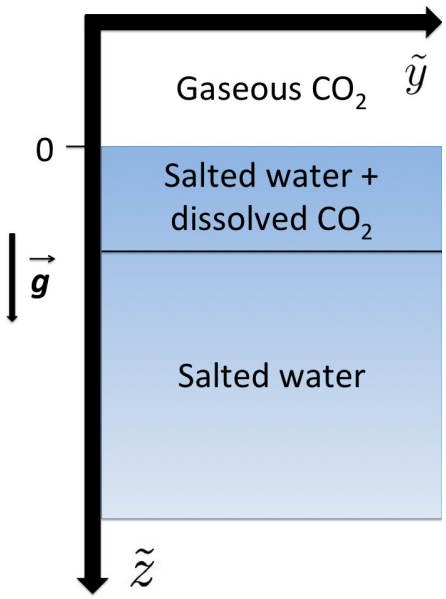

FIG. 1. Two-dimensional model system: gaseous CO_2 dissolves in salted water from the upper boundary of the aqueous solution, located at $\tilde{z} = 0$.

phase coupled with a hydrocarbon liquid phase, most studies consider the aqueous phase only, with a fixed CO_2 concentration at the interface. Similarly, our model focuses on the aqueous solution, which is supposed to be semi-infinite, i.e. to extend from $-\infty$ to $+\infty$ along the horizontal axis $\tilde{y}$ and from 0 to $+\infty$ downwards along the vertical axis $\tilde{z}$.

Experiments in Hele-Shaw cells are usually conducted at low pressures of CO_2 of the order of atmospheric pressure, and at room temperature. We therefore assume that the corresponding low aqueous concentrations of CO_2 (< 0.5 mol/L) do not affect significantly the viscosity of the solution which is taken as constant. Experiments and simulations show that the diffusion coefficient of CO_2 does not depend on the pressure of CO_2 up to 100 bars, although it depends on temperature and salt concentration[15–17]. The solvent is treated as incompressible and we make the Boussinesq approximation[5]. The only density changes in the system are due to the solutal contributions of both CO_2 and salt. The system is considered as isothermal to focus on the solutal contribution of CO_2 dissolution on the density field. This assumption is reasonable as Javaheri, Abedi, and Hassanzadeh [18] have shown that the effect of geothermal gradients can be neglected in front of solutal effects in real sites for CO_2

sequestration.

To describe the dynamics in the aqueous layer, we use the incompressible Darcy's equations (1a, 1b) for the flow field and a diffusion-convection equation (1c) governing the evolution of the concentration field of dissolved CO_2. These two equations are coupled via an equation of state for the density of the solution (1d):

$$\tilde{\boldsymbol{\nabla}}\tilde{p} \;=\; -\frac{\mu}{\kappa}\,\tilde{\mathbf{u}} + \tilde{\rho}\,\mathbf{g}\,, \tag{1a}$$

$$\tilde{\boldsymbol{\nabla}}\cdot\tilde{\mathbf{u}} \;=\; 0\,, \tag{1b}$$

$$\phi\,\frac{\tilde{\partial}\tilde{A}}{\tilde{\partial}\tilde{t}} + (\tilde{\mathbf{u}}\cdot\tilde{\boldsymbol{\nabla}})\,\tilde{A} \;=\; \phi\,D\,\tilde{\nabla}^2\,\tilde{A}\,, \tag{1c}$$

$$\tilde{\rho} \;=\; \tilde{\rho}_0 + \rho_w\,\alpha_A\,\tilde{A}\,, \tag{1d}$$

where $\tilde{p}$ is the pressure, $\tilde{\mathbf{u}} = (\tilde{u}, \tilde{v})$ the fluid velocity, $\tilde{\rho}$ the density, $\tilde{A}$ the concentration of CO_2, and $\tilde{t}$ is the time. The tilde on these variables denote dimensional variables. In addition, μ is the dynamic viscosity, ϕ the porosity, κ the permeability, $\mathbf{g} = (0, g)$ the acceleration due to gravity, D the molecular diffusion coefficient of CO_2 in the solution, ρ_w the density of pure water, and $\alpha_A = \frac{1}{\rho_w}\frac{\tilde{\partial}\tilde{\rho}}{\tilde{\partial}\tilde{A}}$ is the solutal expansion coefficient of CO_2 and $\tilde{\rho}_0$ is the density of the salted water.

Initially, $\tilde{\mathbf{u}}$ and $\tilde{A}$ are zero everywhere in the aqueous solution, except at the interface where, due to local equilibrium with the gaseous phase, $\tilde{A}$ is fixed by Henry's law $m_A = p_{CO_2}/H_{CO_2}$. Here, m_A is the solubility of CO_2 expressed in molality (mol/kg), H_{CO_2} is Henry's constant and p_{CO_2} is the partial pressure of gaseous CO_2, assumed to be maintained constant. Henry's constant depends on temperature and salt concentration as detailed in Appendix A (Eq. (A6)). As the interface is supposed to remain fixed, we impose $\tilde{v} = 0$ at $\tilde{z} = 0$. At $\tilde{z} \to \infty$, we impose $\tilde{v}$ and $\tilde{A} \to 0$ as boundary conditions.

We nondimensionalise the variables as $A = \tilde{A}/A_0$, $\boldsymbol{z} = \tilde{\boldsymbol{z}}/l_c$, $t = \tilde{t}/t_c$, $\boldsymbol{u} = \tilde{\boldsymbol{u}}/u_c$, $\rho = \frac{\tilde{\rho}-\tilde{\rho}_0}{\Delta\rho}$, where $\Delta\rho = \tilde{\rho}(\tilde{z}=0) - \tilde{\rho}_0 = \rho_w\,\alpha_A\,A_0$ is the density difference between the solution saturated with CO_2 and the initial solution with no CO_2. The ambient pressure $\tilde{p}_a$ and the hydrostatic pressure $\tilde{\rho}_0\,g\,\tilde{z}$ are used to define a dimensionless dynamic pressure $p = \frac{\tilde{p}-\tilde{p}_a-\tilde{\rho}_0\,g\,\tilde{z}}{p_c}$. We choose the hydrodynamic velocity, time, pressure and length scales, given by

$$p_c = \frac{\mu\,D\,\phi}{\kappa}, \quad u_c = \frac{\Delta\rho\,g\,\kappa}{\mu}, \quad t_c = \frac{\phi^2\,D}{u_c^2}, \quad l_c = \frac{\phi\,D}{u_c}. \tag{2}$$

As the flow is incompressible, the streamfunction Ψ formulation is employed for conve-

nience. Using $u = -\Psi_z$ and $v = \Psi_y$ gives the parameter-free dimensionless model

$$\nabla^2 \Psi = A_y, \tag{3a}$$

$$A_t - \Psi_z A_y + \Psi_y A_z = \nabla^2 A, \tag{3b}$$

$$\rho = A, \tag{3c}$$

with $\nabla^2 = \frac{\partial^2}{\partial y^2} + \frac{\partial^2}{\partial z^2}$ and subscripts denote derivative as for instance $f_x = \frac{\partial f}{\partial x}$. The boundary conditions read

$$z = 0 : A = 1,\ \Psi = 0; \tag{4a}$$

$$z \to \infty : A \to 0,\ \Psi \to 0, \tag{4b}$$

while the initial conditions are

$$A(z = 0) = 1, \quad A(z > 0) = 0; \tag{5a}$$

$$\Psi = 0. \tag{5b}$$

III. LINEAR STABILITY ANALYSIS (LSA)

On the basis of Eqs. (3a)-(3b), a LSA can be performed to obtain dispersion curves giving the growth rate of the perturbations as a function of the wavenumber. In our case, the LSA is performed using a Quasi-Steady State Approximation, assuming that the diffusive base state does not change significantly on the typical time of growth of the perturbation[19]. We note that other LSA methods[20] can be used as well to provide theoretical predictions. The next step is to switch from these dimensionless predictions towards dimensional results to be compared to experiments. Our methodology for this step is independent of the chosen method of LSA.

In the absence of any flow ($\Psi = 0$), the analytical time-dependent concentration base state A^s, solution of Eq. (3b) in a semi-infinite system (i.e. with boundary conditions (4)) reads:

$$A^s(z,t) = 1 - \mathrm{erf}\left(\frac{\mathrm{z}}{2\sqrt{\mathrm{t}}}\right). \tag{6}$$

Figure 2 shows that, as $\rho^s(z,t) = A^s(z,t)$, dissolved CO_2 increases the density of the aqueous solution, creating a denser layer above pure salted water, the extent of which increases with

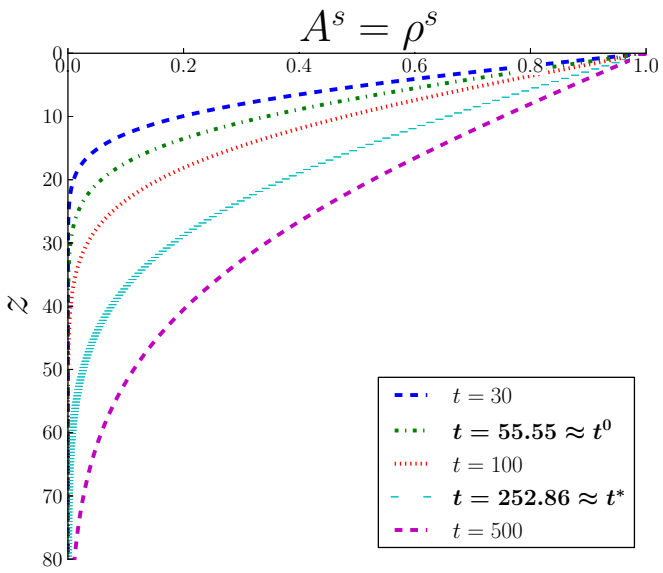

FIG. 2. (Color online) Diffusive concentration profiles of CO_2 given by Eq.(6) or density profiles at increasing times from top to bottom. The two times written in bold are the onset time t^0 and the characteristic time t^* defined in sections IV B and IV C.

time. Beyond a certain time, the denser layer is large enough to trigger a buoyancy-driven instability.

The LSA consists in adding perturbations of ampitude a or ψ to the base state solution at a frozen time t_f, characterized by the concentration profile (6) and $\Psi^s = 0$ as $(A, \Psi) = (A^s, 0)(z, t_f) + (a, ik^{-1}\psi)(z) \exp(\sigma\, t + i\, k\, y)$, where $i^2 = -1$, k is the wavenumber of the perturbation and σ its growth rate[21]. The linearised evolution equations for the disturbances a and ψ are thus

$$\psi_{zz} - k^2\psi = k^2 a, \tag{7a}$$

$$\sigma a - \psi A^s_z = a_{zz} - k^2 a, \tag{7b}$$

The boundary conditions for the disturbances are

$$z = 0 : a = 0,\ \psi = 0, \tag{8a}$$

$$z \to \infty : a \to 0,\ \psi \to 0. \tag{8b}$$

We solve Eq.(7) with boundary conditions (8) numerically on a discrete set of points, with the second-order derivatives approximated by finite differences[21,22]. We check the accuracy

of our numerical scheme by varying the domain size and refining the mesh. The domain size L is taken large enough to effectively replace condition (8b) by $a = 0, \psi = 0$ at $z = L$. Typical values for L and the mesh size to achieve an accuracy of 0.1% in the computation of the maximum growth rates are 500 and 0.20, respectively. We note that for growth rates corresponding to small wavenumbers (typically smaller that 0.005), L must be at least four times larger to reach sufficient convergence. We also check that the numerical dispersion curve of the initial condition (5) converged to the analytical dispersion curve[23] $\sigma = -k^2$ and that the numerical dispersion curve of a step function converged to the one predicted analytically[24].

IV. CHARACTERISTICS OF THE INSTABILITY

A. Dimensionless universal dispersion curve

Figure 3 shows dimensionless dispersion curves computed numerically for the base state profiles (6). For small values of t, all growth rates are negative, which means that the system remains stable. This is coherent with the fact that, initially, CO_2 diffuses without convection as observed experimentally[1,6,7]. After some time, however, CO_2 accumulates in the aqueous layer and increases the unfavorable density stratification in the gravity field. A band of wavenumbers have their associated growth rate that becomes positive, which is the sign of instability as the related perturbations are then growing exponentially in time. The time when the maximum growth rate of the dispersion curve, σ_m, becomes positive, is defined as the onset time t^0. Figure 4(a) shows that the maximum growth rate of the dispersion curve, σ_m, increases in time up to a maximum value and then decreases. This decrease is related to a weakening of the unstable density gradient by diffusion as time goes by. The wavenumber k_m associated to the maximum growth rate also varies non monotonically as a function of time as shown in figure 4(b).

B. Onset time t^0 and wavenumber k_m^0

Most previous papers devoted to a LSA of CO_2 dissolving into water have characterized the buoyancy-driven instability by the onset time t^0 at which $\sigma_m = 0$, beyond which the system thus becomes unstable, and by the related onset wavenumber k_m^0. In our case, the

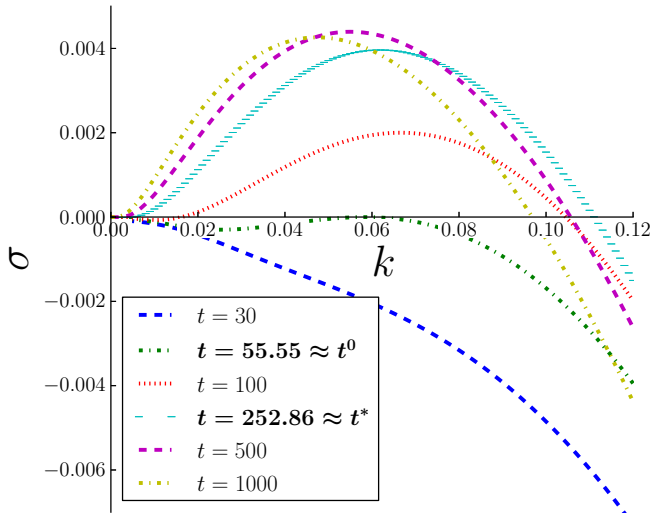

FIG. 3. (Color online) Dimensionless dispersion curves characterizing the stability of the diffusive profiles given by Eq.(6) at various times.

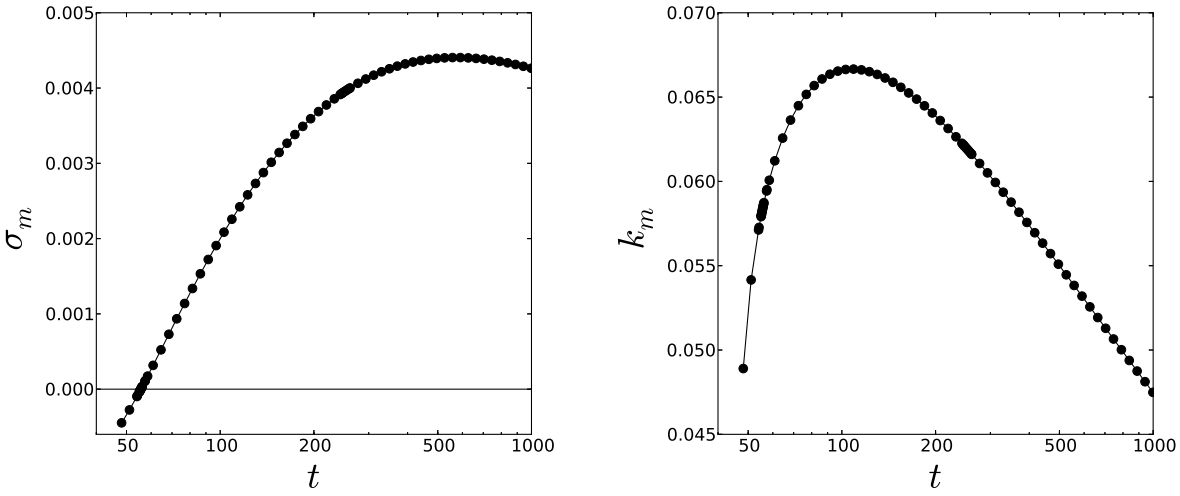

(a) (b)

FIG. 4. (a) Maximum growth rate σ_m of the dispersion curves of figure 3, as a function of time. (b) Wavenumber k_m associated to σ_m, as a function of time.

onset characteristics are

$$\sigma_m^0 \;=\; (0.000 \pm 0.004) \times 10^{-3}, \quad t^0 = 55.59 \pm 0.07, \tag{9a}$$

$$k_m^0 \;=\; (5.83 \pm 0.01) \times 10^{-2}, \quad \lambda_m^0 = 2\pi/k_m^0 = 107.7 \pm 0.2. \tag{9b}$$

These onset time and wavenumber are in good agreement with those found in several previous theoretical studies[25–31]. Additionally, these onset characteristics are close to those evaluated experimentally in systems analogous to the CO_2/water system[9,11]. Backhaus, Turitsyn, and Ecke[11] also measured the ratio between the vertical length of the fingers and their wavelength at the onset of the instability. To evaluate this ratio here, we suppose the concentration profile at the onset of the instability is still close to the analytical profile (6). We use that profile (6) to define the length of the fingers as the length over which the dimensionless diffusive CO_2 concentration is larger or equal to 0.01. We found a ratio, 0.25, in good agreement with the experimental values reported to be between 0.22 and 0.27[11] and with the value we extract from Ref.32.

C. Characteristic growth rate σ^*

The onset time t^0 (and the related wavenumber k_m^0) of the instability are difficult to determine experimentally as perturbations are then so small that the dynamics remains mainly diffusive. To compare LSA results to experimental measurements in the linear regime as done by various authors[1,33,34], it is of interest to predict a characteristic growth rate σ^* of the instability quantifying the rate at which fingers grow out of the diffusive base profile once the system is unstable.

Following Trevelyan et al.[21], we compute the growth rate σ_m^* as the one for which $\sigma_m^*\, t^* = 1$ such that the amplification factor $\exp(\sigma_m^*\, t^*)$ of the perturbation at t^* is of order unity. For this definition, we find the following characteristic values:

$$\sigma_m^* \;=\; (3.96 \pm 0.02) \times 10^{-3}\,, \quad t^* = 252 \pm 2 \tag{10a}$$

$$k_m^* \;=\; (6.192 \pm 0.009) \times 10^{-2}\,, \quad \lambda_m^* = 2\pi/k_m^* = 101.5 \pm 0.1. \tag{10b}$$

The growth rate σ_m^* is of the same order of magnitude as that we estimate from figure 6 of Riaz et al.[32] and as those estimated by Slim et al.[9] and Elenius et al.[35].

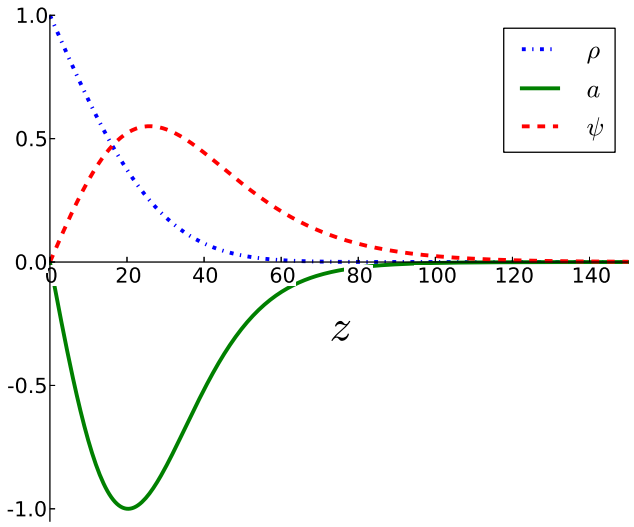

FIG. 5. $a(z)$ and $\psi(z)$, amplitude of the perturbations of the concentration and the streamfunction, at the characteristic time t^* and wavenumber k_m^*, along with the base state density profile $\rho^s(z, t^*)$.

Figure 5 shows that, at this time t^*, the convective rolls have their largest amplitude at a given distance below the gas-liquid interface, in good agreement with experimental observations[1,6,7,9].

D. Dimensional scales

Most LSAs stop at this stage and refrain from direct comparison with laboratory-scale experiments. This comparison is indeed not trivial to perform as results (10) are free of any experimental parameter and need to be dimensionalised back as:

$$\tilde{\sigma}^* = \sigma^*/t_c; \qquad \tilde{\lambda}^* = \lambda^* \, l_c, \tag{11}$$

where the characteristic scales

$$l_c = \frac{D\mu\,\phi}{\Delta\rho\, g\, \kappa}; \qquad t_c = \frac{l_c^2}{D} \tag{12}$$

are specific to each experiment. We insist on the fact that these scales are independent of the length of the experimental set-up, and are intrinsic to the porous medium (porosity ϕ, permeability κ), to the liquid at hand (viscosity μ) and to the properties of CO_2 dissolved

in the solvent (diffusion coefficient D and difference of density $\Delta\rho$). We thus see that the parameters that are typically varied in laboratory-scale experiments such as the pressure p_{CO_2} of CO_2, the salt concentration B_0, and the temperature T do not appear explicitly in (12). Their effect on the spatial and time scales - and thus on the characteristic growth rate and wavelength of the fingering pattern - is implicit and not trivial to characterize. Our goal here is to show how to estimate these characteristics as a function of the control parameters to allow a direct comparison between theoretical predictions and experiments.

The various parameters involved in the characteristic scales (12) implicitly depend on B_0, T, and p_{CO_2}. We review these dependences below. The first two characteristics - porosity and permeability - depend only on the nature of the porous medium and are constant for a given experimental set-up. The viscosity μ of the aqueous solution and the diffusion coefficient D on the other hand both depend on B_0 and T, but not on p_{CO_2} as explained in section II. Increasing B_0 hinders CO_2 transport (as this increases μ and decreases D) because of the interactions of the solvent with the salt ions. Increasing T on the contrary improves the transport (decreases μ and increases D) because it increases the thermal molecular motion.

Eventually, the implicit dependence of $\Delta\rho$ on B_0 and T is even more tricky as these parameters affect the solubility A_0 of CO_2, the density ρ_w of water and the solutal expansion coefficient α_A of CO_2 which all come into play in $\Delta\rho$. ρ_w depends on temperature (see Eq. (A8)) and does not vary significantly with pressure over the range of pressures studied here[36] (1-5 atm). α_A is also assumed to depend only on temperature[37]. A_0, however, depends on CO_2 pressure, salt concentration and temperature. Indeed, all three parameters influence the equilibrium between the gaseous CO_2 and the dissolved CO_2.

We propose in Appendix A correlations to compute all implicit dependences of μ, D, and $\Delta\rho$ on B_0 and T to compare our theoretical predictions with results obtained from experiments in Hele-Shaw cells[1,6,7]. On the basis of these correlations, we discuss now the explicit influence of CO_2 pressure, salt concentration and temperature on the development of the buoyancy-driven instability.

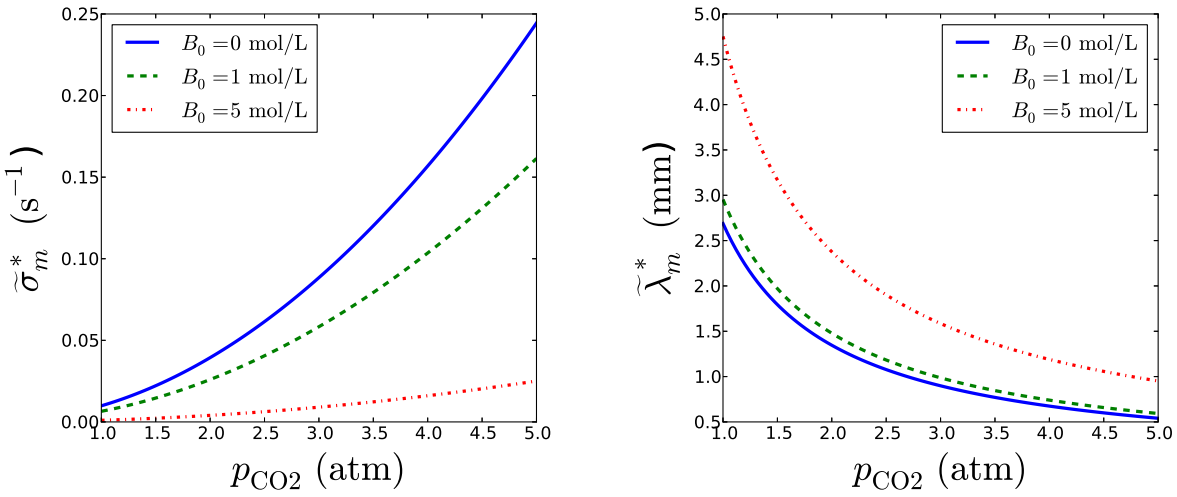

(a) (b)

FIG. 6. Characteristic dimensional (a) growth rate $\tilde{\sigma}_m^*$ in s^{-1}, and (b) wavelength $\tilde{\lambda}_m^*$ in mm as a function of p_{CO_2}, the pressure of CO_2 in atm, at $T = 26$°C for various concentrations B_0 of NaCl.

V. INFLUENCE OF EXPERIMENTAL PARAMETERS ON THE CHARACTERISTICS OF THE INSTABILITY

A. Pressure of CO_2

Inspired by recent experiments[1], we vary the pressure of CO_2, p_{CO_2}, between 1 and 5 atm for various salt concentrations B_0, while the temperature T is kept constant at 26°C. The salt chosen here is pure NaCl.

Figure 6 shows that the growth rate $\tilde{\sigma}_m^*$ increases and the wavelength $\tilde{\lambda}_m^*$ decreases (i.e. k_m^* increases) with p_{CO_2}. The system becomes thus more unstable when CO_2 pressure is increased. This can be related to the increase of the solubility of CO_2, A_0, which is proportional to the pressure of CO_2 (see section II). Consequently, the unfavorable density gradient responsible for the onset of the instability increases, as can be seen in figure 7. Figure 7 also shows that a density difference $\Delta\rho = \tilde{\rho}(\tilde{z} = 0) - \tilde{\rho}_0$ as small as 0.3 g/L can be large enough to trigger the instability.

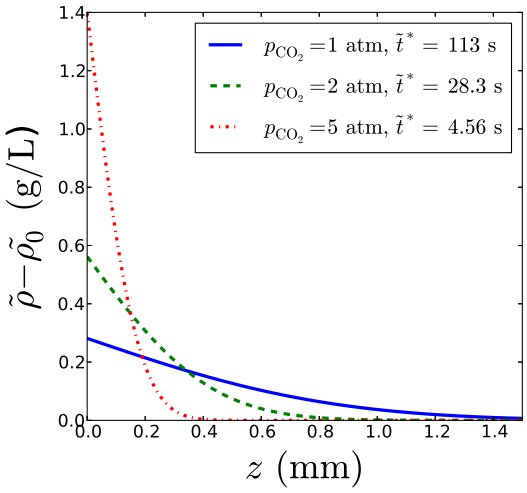

FIG. 7. Density profiles $\tilde{\rho} - \tilde{\rho}_0$ in g/L computed from Eq. (6) for $B_0 = 0$ mol/L, $T = 26$°C, and various pressures p_{CO_2} of CO_2, at the same dimensionless characteristic time t^* (Eq. (10a)) corresponding to different dimensional times $\tilde{t}^*$.

B. NaCl concentration

The amount of NaCl dissolved in the water, B_0, impacts several physico-chemical characteristics defining the length and time scales needed to redimensionalise our predictions (see explicit formulas in Appendices A and B). These characteristics are the diffusion coefficient D of CO_2, the viscosity μ of the solution, and the solubility A_0 of CO_2 needed to compute $\Delta\rho$. The global effect of B_0 on the length and time scales is therefore not intuitive to predict. We thus vary B_0 between 0 mol/L and 5 mol/L for various pressures of CO_2 while the temperature T is kept constant at 26°C.

Figure 8 shows that the growth rate $\tilde{\sigma}_m^*$ decreases while the wavelength $\tilde{\lambda}_m^*$ increases slightly (i.e. k_m^* decreases) with B_0. Increasing the concentration of NaCl thus stabilizes the system with regard to buoyancy-driven convection. We explain this stabilization by the effect of B_0 on μ and A_0 being larger than the effect of B_0 on D. The decrease of D with B_0 tends to destabilize the system as diffusion smoothes the unstable concentration profile. On the contrary, the increase of μ with B_0 stabilizes the system because viscosity hinders the transport of flow. Figure 9 shows that the decrease of the solubility A_0 of CO_2 with the concentration B_0 of salt (see Eq. (A5)-(A6)) decreases the density difference $\Delta\rho$ at the

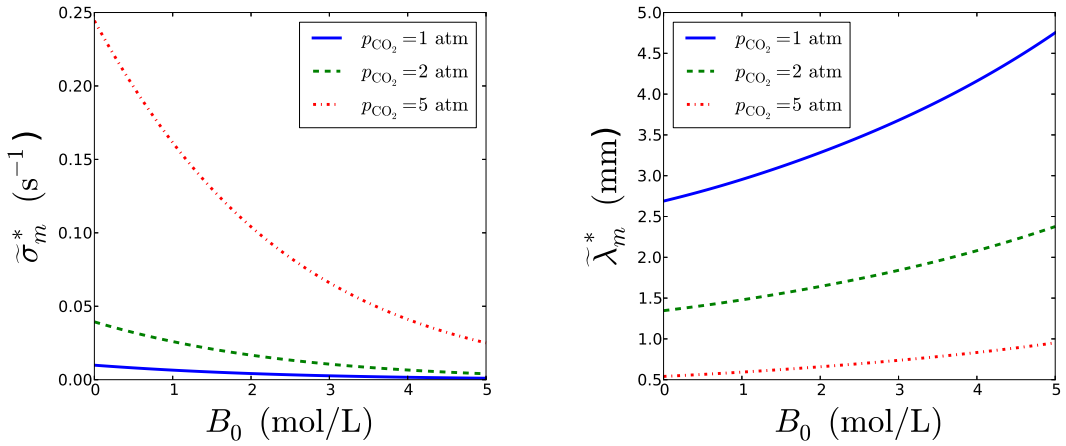

(a) (b)

FIG. 8. Characteristic dimensional (a) growth rate $\tilde{\sigma}_m^*$ in s^{-1} and (b) wavelength $\tilde{\lambda}_m^*$ in mm as a function of the concentration of NaCl, B_0 in mol/L, at $T = 26^{\circ}$C for various pressures of CO_2, p_{CO_2} in atm.

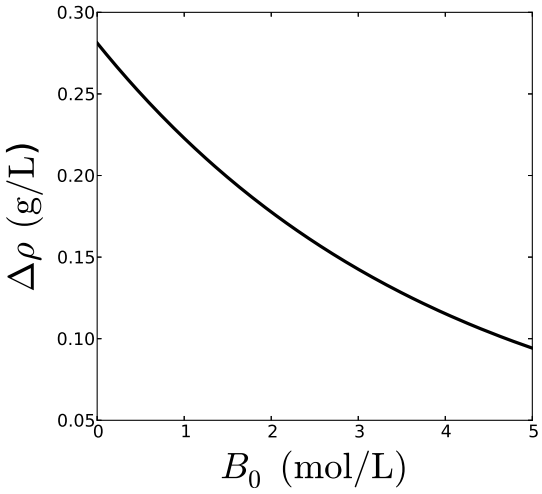

FIG. 9. Difference of density between the solution saturated with CO_2 and the initial solution with no CO_2 as a function of the concentration of NaCl, B_0 in mol/L, for $p_{CO_2} = 1$ atm and $T = 26^{\circ}$C.

origin of the instability and thus also stabilizes the system.

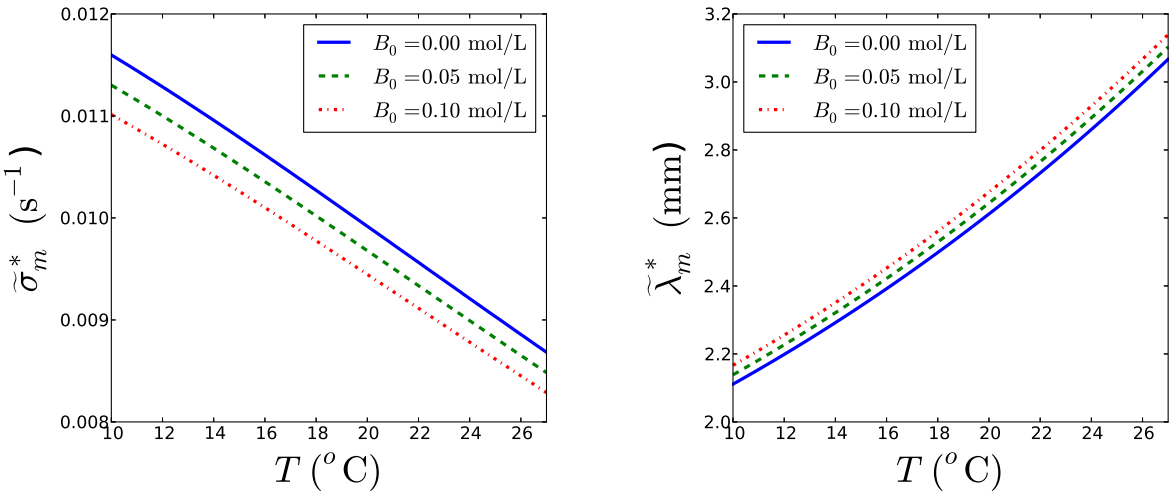

FIG. 10. Characteristic dimensional (a) growth rate $\tilde{\sigma}_m^*$ in s^{-1} and (b) wavelength $\tilde{\lambda}_m^*$ in mm as a function of temperature T, at $p_{CO_2} = 1$ atm for various concentrations of NaCl, B_0 in mol/L.

C. Temperature

The temperature T of the system impacts even more physico-chemical characteristics than the salinity. It influences not only D, μ, and A_0, but also the density of water ρ_w and the solutal expansion coefficient of CO_2, α_A. The impact of T on the instability is thus clearly not intuitive. To explicit it, we vary the temperature from 10 to 27 °C for various concentrations of NaCl at $p_{CO_2} = 1$ atm and for various pressures of CO_2 at $B_0 = 0$ mol/L. As we could not find any empirical correlation for D that takes simultaneously into account T and B_0, we choose low concentrations of NaCl to assume that D and μ are the same as in pure water.

Figure 10 shows that increasing the temperature stabilizes the system as $\tilde{\sigma}_m^*$ decreases and $\tilde{\lambda}_m^*$ increases. The stabilization of the system with temperature can be explained by the effect of T on D, ρ_w and A_0 being larger than that on μ and α_A. In particular, figure 12 shows that although α_A increases with T, the global effect of increasing temperature is to reduce the density difference $\Delta\rho$.

We note, however, that changes in the absolute values are much smaller than those induced by a change of pressure (Fig.6) or salinity (Fig.8) and are in the range of typical

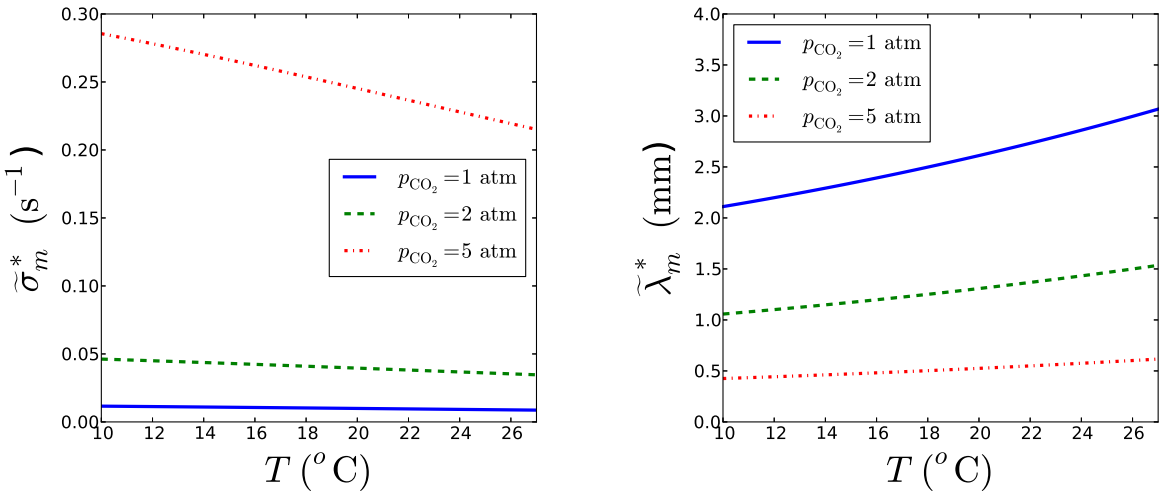

(a) (b)

FIG. 11. Characteristic dimensional (a) growth rate $\tilde{\sigma}_m^*$ in s^{-1} and (b) wavelength $\tilde{\lambda}_m^*$ in mm as a function of temperature T, at $B_0 = 0$ mol/L for various pressures of CO_2, p_{CO_2} in atm.

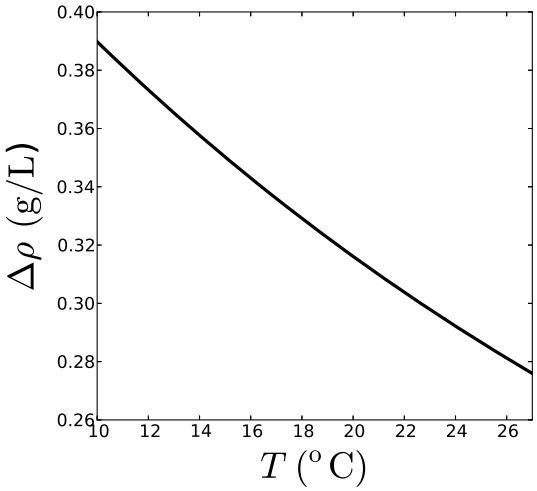

FIG. 12. Difference of density between the solution saturated with CO_2 and the initial solution with no CO_2 as a function of temperature T, for $p_{CO_2} = 1$ atm and $B_0 = 0$ mol/L.

experimental errors. This is rather counter-intuitive since the temperature affects most of the physical quantities of the problem. As an example, at $B_0 = 0$ mol/L and $p_{CO_2} = 1$ atm, between 20°C and 25°C, which correspond to two different typical room temperatures, the wavelength varies between 2.5 and 2.8 mm only. Provided that the whole set-up is at the

same room temperature, it seems therefore not crucial to control the temperature of the set-up with a thermostat if the temperature changes by only a few degrees. Figure 11 shows that these trends hold for different pressures of CO_2 as well.

D. Comparison with experiments

Only few laboratory-scale experiments have characterized the convective dissolution of CO_2 in salted water. Farajzadeh *et al.*[2] showed that the rate of the mass transfer of CO_2 to an aqueous solution is larger than that predicted in a purely diffusive case. This confirms that the buoyancy-driven convection developing upon CO_2 dissolution plays an important role in the transport of dissolved CO_2. They also evaluated the effect of the pressure of CO_2, of the presence of a salt (NaCl) and of the concentration of a surfactant on the transfer rate of CO_2. This transfer rate increases with p_{CO_2} and decreases when NaCl is added. We explain this result with the fact that the growth rate of the instability increases with p_{CO_2} (Fig.6a) and decreases with the concentration of NaCl (Fig.8a). As convection transports CO_2 away from the interface more efficiently, any parameter that increases the growth rate of the convective instability will increase the transfer rate of CO_2 to the aqueous solution.

Other studies have explicitly measured the wavelength and/or the growth rate characterizing the buoyancy-driven instability in the CO_2/water system. Outeda *et al.*[1] showed that the growth rate of the instability increases with the pressure of CO_2, which is coherent with our predictions. From a quantitative point of view, this increase is slower than predicted. For example, for $T = 20^oC$, $p_{CO_2} = 2$ atm, and a gap width of 1 mm, Outeda *et al.*[1] measured a growth rate of 0.17 s^{-1}, while we predict $\tilde{\sigma}_m^* = 0.63$ s^{-1}. However, if we account for an experimental error of 10 % in the gap width, our predicted $\tilde{\sigma}_m^*$ can be reduced to 0.41 s^{-1}. We also note that Darcy's law might be overestimating the growth rate for such a large gap[38]. In a similar system, at $T = 22^oC$, $p_{CO_2} = 1$ atm, and $\kappa = 4.08 \times 10^{-8}$ m^2, Kneafsey and Pruess[6] measured a wavelength of 10 mm when they first saw fingers, while we predict that $\tilde{\lambda}_m^*$ is 1.4 mm but can be as large as 1.7 mm if we account for an experimental error of 10% in the gap width.

Even if our theoretical predictions allow to interpret the trends observed experimentally[1,2], we note that the exact quantitative comparison faces two problems. First, as pointed out by Riaz et al.[32], it is unclear at what time exactly buoyancy-driven fingering becomes observable

in the experiment. We evaluate indeed a characteristic time $\tilde{t}_m^*$ of 71 s for the experiment of Kneafsey and Pruess[6], which is smaller than the time where they first observed fingers, i.e. 180 s. Similarly, in the experiment of Outeda *et al.*[1] at $p_{CO_2} = 1.5$ atm, fingers are first observed at 60 s, while we predict that $\tilde{t}_m^*$ is 2.8 s only. Since the instability could have started before the first fingers are observed, we suggest, in further experiments, to measure the growth rate of the instability by quantifying the difference between the measured concentration profile and the predicted diffusive one[9].

Second, the time at which fingers are observed experimentally depends on the visualization technique used. All experiments cited here use a pH indicator to visualize the dynamics of dissolved CO_2[1,6,7]. In that case, the change of color is related to a given pH threshold, which does not necessarily follow the contour of the finger. In addition, instead of being a mere visualization mean, a pH indicator can have a dramatic effect on hydrodynamic instabilities as its presence can affect the density profile[39,40]. This is indeed likely in the CO_2 experiments[1,6,7] as Outeda et al.[1] reported that varying the concentration of the pH indicator affects the growth rate of the instability. We therefore suggest that future experiments devoted to benchmark theoretical predictions should be done without the use of pH indicators[41].

VI. CONCLUSION

In the context of CO_2 sequestration, experimental studies of dissolution-driven convective instabilities in Hele-Shaw cells have regained interest. Indeed, convection enhances the mass transfer of CO_2 in the aqueous solution, thereby improving the safety of the sequestration. The benchmarking of theoretical predictions remains, however, difficult because of the use of dimensionless parameter-free models. Using a linear stability analysis, we have thus predicted the explicit effect of experimental control parameters on the buoyancy-driven instability that develops when CO_2 dissolves at the top of an aqueous solution. To do so, we have dimensionalized the theoretical LSA predictions, by using the dependence of time and length scales of the problem on CO_2 pressure, salt concentration and temperature. We note that the procedure used here can easily be applied to dimensionalize back other results obtained with different theoretical methods.

We have studied the influence of experimental parameters on the short-time characteris-

tics of the instability: the onset time $\tilde{t}^0$ and wavenumber $\tilde{k}_m^0$, and the characteristic growth rate $\tilde{\sigma}_m^*$ and wavenumber $\tilde{k}_m^*$. We have explained the destabilizing effect of CO_2 pressure by its impact on the solubility of CO_2 in the aqueous solution. By contrast, the stabilizing effect of salt concentration or temperature on the instability is less intuitive as both parameters implicitly impact several physical quantities appearing in the time and length scales. These predicted effects are coherent with experimental trends[1,2]. We also show that the characteristics of the instability are not much sensitive to changes of room temperature by a few degrees, so that experimental results should be robust without a need to place the set-up in a thermostat.

Our study paves the way to future benchmarking of theoretical predictions with laboratory-scale experiments. Our model could easily be applied to study the influence of other dissolved salts than NaCl as encountered in geological systems. It could also be developed to take into account the non ideality of the solutions, as most certainly is the case in sequestration sites, where pressure and temperature are higher. A study of the effect of chemical reactions on the convection has been undertaken.

ACKNOWLEDGMENTS

We thank A. D'Onofrio, A. Zalts, P.M.J. Trevelyan, J.-L. Tison, B. Delille and K. Loos for fruitful discussions. V.L. is Research Fellow of the Fonds de la Recherche Scientifique-FNRS. This source of funding is gratefully acknowledged. A.D. acknowledges financial support from FNRS Forecast project, Prodex, Fonds Defay and ARC CONVINCE.

Appendix A: Empirical correlations for physical properties

We describe here the correlations used to compute the length and time scales, l_c and t_c respectively, needed to dimensionalise back the theoretical predictions and give some realistic values for experiments in Hele-Shaw cells conducted at low pressures of CO_2 and room temperature. As $l_c = D\mu\,\phi/\Delta\rho\,g\,\kappa$ and $t_c = l_c^2/D$, we need to evaluate the porosity ϕ, the permeability κ, the dynamic viscosity μ and the molecular diffusion coefficient D of CO_2 in water. The gap width of the Hele-Shaw cell b, the temperature T, the concentration of the salt dissolved in water B_0, and the pressure p_{CO_2} of CO_2 are given by the experimental

conditions.

In a Hele-Shaw cell, the porosity ϕ is equal to one. The permeability, $\kappa = b^2/12$, is evaluated as 2.08 $\times 10^{-8}$ m^2 for a cell of thickness $b = 0.5$ mm. The gravity acceleration is $\cos(\beta)$ 9.81 m/s^2 where β is the angle between the vertical and the orientation of the cell.

To compute the dynamic viscosity μ of the solution in mPa.s for a given salt concentration and temperature, we use the empirical expression[42]:

$$\mu = \mu_w^{w_w} \prod_{i=1}^{n} \mu_i^{w_i} , \tag{A1}$$

where w_w is the mass fraction of water in the solution, w_i is the mass fraction of the solute i in the solution computed from the concentration with Eq. (B3), and n is the total number of solutes dissolved in water. μ_w is the viscosity of water and μ_i is the contribution of the solute i to the viscosity. μ_w in mPa.s is computed as a function of the temperature T in °C with the empirical expression[42]:

$$\mu_w = \frac{T + a_3}{a_2\, T^2 + a_1\, T + a_0} , \tag{A2}$$

with $a_3 = 246$ °C, $a_2 = 0.05594$ °C^{-1} mPa^{-1} s^{-1}, $a_1 = 5.2842$ mPa^{-1} s^{-1} and $a_0 = 137.37$ °C mPa^{-1} s^{-1}. For example, using formula (A2), we find that the viscosity of water is 1.002 mPa.s at 20 °C. μ_i is computed from Ref.42 as:

$$\mu_i = \frac{\exp\left(\frac{\nu_1\,(1-w_w)^{\nu_2}+\nu_3}{\nu_4\, T+1}\right)}{\nu_5\,(1-w_w)^{\nu_6}+1} . \tag{A3}$$

For NaCl, $\nu_1 = 16.222$, $\nu_2 = 1.3229$, $\nu_3 = 1.4849$, $\nu_4 = 0.0074691$ °C^{-1}, $\nu_5 = 30.78$, and $\nu_6 = 2.0583$.

We have not found an empirical correlation taking simultaneously into account the dependence of the diffusion coefficient of CO_2 on temperature and salt concentration. Therefore, we use two different exponential correlations of the type

$$D = a\, \exp(b\, X). \tag{A4}$$

The dependence of D on temperature T is computed by a regression of experimental data giving the diffusion coefficient of CO_2 in pure water as a function of T[36]. In this case, $a = 9.6861 \times 10^{-10}$ m^2/s, $b = 0.02691$ °C^{-1}, and $X = T$ in °C.

The dependence of D on the concentration of NaCl, B_0 in mol/L, follows the empirical correlation (A4) at 26°C with $a = 1.75 \times 10^{-9}$ m/s^2, b = -0.229 (mol/L)$^{-1}$, and $X = B_0$ in mol/L[15].

We note that we can use both empirical regressions (A4) to calculate the diffusion coefficient of CO_2 at $T = 26$°C and $B_0 = 0$ mol/L. The obtained values differ by about 10% probably because of uncertainties in the different methods of measurement of both studies.

To compute the difference in density $\Delta\rho$ between the pure aqueous solution and the aqueous solution saturated with CO_2, we need to know the solubility of CO_2, the density of the aqueous solution and the solutal expansion coefficient of CO_2.

First, the solubility of CO_2 in the aqueous solution is computed using Henry's law

$$m_A = p_{CO_2}/H_{CO_2}\,, \tag{A5}$$

where m_A is the molality of CO_2 in the liquid phase, p_{CO_2} is the partial pressure of CO_2 in the gas phase, and H_{CO_2} is Henry's constant. This expression is valid for the ranges of pressure, temperature and salt concentration that we are studying[43]. We used the following empirical correlation for the dependence of the dimensionless Henry's constant $\hat{H}_{CO_2} = H_{CO_2}/$ (10^6 Pa kg/mol) on the temperature and the composition in salt:

$$\begin{aligned}\ln \hat{H}_{CO_2} = (192.876 + 0.024125\,\hat{m}_B - 0.00752\,\hat{m}_B^2)\\ +(-9624.4 + 0.000199\,\hat{m}_B)/\hat{T}\\ +(0.01441 - 0.002111\,\hat{m}_B)\,\hat{T}\\ +(-28.749 + 0.1446\,\hat{m}_B)\,\ln\hat{T}\,,\end{aligned} \tag{A6}$$

with the dimensionless temperature $\hat{T} = T$ / (1 K), with T in Kelvin, and the dimensionless molality of NaCl $\hat{m}_B = m_B$ / (1 mol/kg). We use expression (B4) to compute m_B from B_0, the concentration of NaCl. Henry's constant increases with temperature and with the concentration of NaCl, meaning that the solubility of CO_2 decreases with temperature and the concentration of NaCl. Increasing the temperature displaces the equilibrium towards the gas phase while increasing the concentration of NaCl induces a "salting-out" effect probably due to electrostatic interactions.

Second, ρ, the density of the aqueous solution in kg/m^3, is computed from the mass fraction of solute i, w_i, as[44]

$$\rho = \frac{1}{\frac{1}{\rho_w} + \sum_{i=1}^{n}\left(V_i - \frac{1}{\rho_w}\right) w_i}\,, \tag{A7}$$

with ρ_w the density of water in kg/m^3 and V_i the specific apparent volume of the solute i in m^3/kg. ρ_w is calculated as a function of the temperature T in °C with the empirical

regression[44]:

$$\rho_w = \frac{b_5\,T^5 + b_4\,T^4 + b_3\,T^3 + b_2\,T^2 + b_1\,T + b_0}{1 + b_6\,T}\,, \tag{A8}$$

where b_5 = - 2.8054253 $\times 10^{-10}$ ^{o}C^{-5} kg/m^3, b_4 = 1.0556302 $\times 10^{-7}$ ^{o}C^{-4} kg/m^3, b_3 = - 4.6170461 $\times 10^{-5}$ ^{o}C^{-3} kg/m^3, b_2 = - 0.0079870401 ^{o}C^{-2} kg/m^3, b_1 = 16.945176 ^{o}C^{-1} kg/m^3, b_0 = 999.83952 kg/m^3, b_6 = 0.01687985 ^{o}C^{-1}. V_i reads[44]

$$V_i = \frac{w_i + c_2 + c_3\,T}{(c_0\,w_i + c_1)\exp\left(c_5(T + c_4)^2\right)}. \tag{A9}$$

For NaCl, c_2 = 1.01660, c_3 = 0.014624 ^{o}C^{-1}, c_0 = -0.00433 kg/m^3, c_1 = 0.06471 kg/m^3, c_5 = 10^{-6} ^{o}C^{-2} and c_4 = 3315.6 ^{o}C. To compute the specific apparent volume of CO_2, we used the empirical correlation adapted from Ref.37:

$$V_A = (d_0 + d_1\,T + d_2\,T^2 + d_3\,T^3)/M_{CO_2}, \tag{A10}$$

where M_{CO_2} is the molar mass of CO_2 = 0.04401 kg/mol, d_0 = 37.51 $\times 10^{-6}$ m^3/mol, d_1 = -9.585 $\times 10^{-8}$ m^3/mol ^{o}C^{-1}, d_2 = 8.740 $\times 10^{-10}$ m^3/mol ^{o}C^{-2}, and d_3 = -5.044 $\times 10^{-13}$ m^3/mol ^{o}C^{-3}.

Third, the solutal expansion coefficient of CO_2, α_A in m^3/mol, is computed as

$$\alpha_A = \frac{M_{CO_2}}{\rho_w} - M_{CO_2}\,V_A. \tag{A11}$$

For example, for the following set of parameters: b = 0.50 mm, ϕ = 1.00, pressure of CO_2 = 1.00 atm, concentration of NaCl = 0 mol/L, temperature = 26.0 ^{o}C, we have the following length and time scales : l_c=2.95 $\times 10^{-5}$ m and t_c=4.47 $\times 10^{-1}$ s, respectively.

Appendix B: Expressions for the quantity of a solute in a solvent

In this section, we explain how to convert different types of expressions for the quantity of a solute i in a solvent containing n different solutes: the molality m_i, the mass fraction w_i, the molarity C_i and the mole fraction x_i. M_i is the molar mass of the solute i in kg/mol.

1. Expressing the composition knowing the molality

The mass fraction w_i is computed from the molality m_i by using

$$w_i = \frac{m_i\,M_i}{1 + \sum\limits_{j=1}^{n} m_j\,M_j}\,. \tag{B1}$$

The molarity C_i is computed from the molality m_i by using

$$C_i = \rho \frac{m_i}{1 + \sum_{j=1}^{n} m_j M_j}, \tag{B2}$$

where ρ is the density of the solution calculated with expression (A7) from the mass fraction w_i, computed with expression (B1) from the molality m_i. As most experiments use mol/L as units, Eq.(B2) is used to convert m_A in mol/kg into A_0 in mol/L.

2. Expressing the composition knowing the molarity

The mass fraction w_i is computed from the molarity C_i by using

$$w_i = \frac{C_i M_i}{\rho} \tag{B3}$$

The molality m_i is computed from the molarity C_i as

$$m_i = \frac{C_i}{\rho - \sum_{j=1}^{n} C_j M_j}. \tag{B4}$$

To use all these expressions, the density of the solution must be known as a function of molarity. For a solution with one single solute i, we insert expressions (B3) and (A9) in (A7) to have the following equation for $\rho(C_i)$:

$$P \rho^2 + Q \rho + R = 0, \tag{B5}$$

where

$$\begin{aligned} P &= c_1 e, \\ Q &= M_i C_i \left[(c_0 - c_1) e + \rho_w (c_2 + c_3 T)\right] - \rho_w c_1 e, \\ R &= (M_i C_i)^2 (\rho_w - c_0 e) - M_i C_i \rho_w c_1 e. \end{aligned} \tag{B6}$$

The constants c_0 to c_4 are defined as in (A9), e is $\exp(c_5(T + c_4)^2)$, M_i is the molar mass of the solute i in kg/mol, and ρ_w is the density of the pure solvent in kg/m^3.

REFERENCES

[1]R. Outeda, C. El Hasi, A. D'Onofrio, and A. Zalts, "Experimental aspects of density-driven convection induced by CO_2 dissolution," Chaos **24**, 013135 (2014).

[2]R. Farajzadeh, A. Barati, H. A. Delil, J. Bruining, and P. L. J. Zitha, "Mass transfer of CO_2 into water and surfactant solutions," Petrol. Sci. Technol. **25**, 1493–1511 (2007).

[3]S. Bachu, "CO_2 storage in geological media: Role, means, status and barriers to deployment," Prog. Energ. Comb. **34**, 254–273 (2008).

[4]A. Firoozabadi and P. Cheng, "Prospects for subsurface CO_2 sequestration," AIChE J. **56**, 1398–1405 (2010).

[5]E. Guyon, J.-P. Hulin, L. Petit, and C. Mitescu, *Physical Hydrodynamics* (Oxford University Press, 2001).

[6]T. J. Kneafsey and K. Pruess, "Laboratory flow experiments for visualizing carbon dioxide-induced, density-driven brine convection," Transp. Porous Med. **82**, 123–139 (2010).

[7]T. J. Kneafsey and K. Pruess, "Laboratory experiments and numerical simulation studies of convectively enhanced carbon dioxide dissolution," Energy Procedia **4**, 5114–5121 (2011).

[8]J. A. Neufeld, M. A. Hesse, A. Riaz, M. A. Hallworth, H. A. Tchelepi, and H. E. Huppert, "Convective dissolution of carbon dioxide in saline aquifers," Geophys. Res. Lett. **37**, L22404 (2010).

[9]A. C. Slim, M. M. Bandi, J. C. Miller, and L. Mahadevan, "Dissolution-driven convection in a Hele-Shaw cell," Phys. Fluids **25**, 024101 (2013).

[10]C. Wylock, S. Dehaeck, A. Rednikov, and P. Colinet, "Chemo-hydrodynamical instability created by CO_2 absorption in an aqueous solution of $NaHCO_3$ and Na_2CO_3," Microgravity Sci. Tec. **20**, 171–175 (2008).

[11]S. Backhaus, K. Turitsyn, and R. E. Ecke, "Convective instability and mass transport of diffusion layers in a Hele-Shaw geometry," Phys. Rev. Lett. **106**, 104501 (2011).

[12]V. Loodts, C. Thomas, L. Rongy, and A. De Wit, "Control of convective dissolution by chemical reactions: General classification and application to CO_2 dissolution in reactive aqueous solutions," Phys. Rev. Lett. **113** (2014), 10.1103/PhysRevLett.113.114501.

[13]L. I. Eide and S. Martin, "The formation of brine drainage features in young sea ice," J. Glaciol. **14**, 137–154 (1975).

[14]L. Rongy, K. B. Haugen, and A. Firoozabadi, "Mixing from Fickian diffusion and natural convection in binary non-equilibrium fluid phases," AIChE J. **58**, 1336–1345 (2012).

[15]A. Sell, H. Fadaei, M. Kim, and D. Sinton, "Measurement of CO_2 diffusivity for carbon sequestration: A microfluidic approach for reservoir-specific analysis," Environ. Sci.

Technol. **47**, 71–78 (2013).

[16]J. W. Mutoru, A. Leahy-Dios, and A. Firoozabadi, "Modeling infinite dilution and Fickian diffusion coefficients of carbon dioxide in water," AIChE J. **57**, 1617–1627 (2011).

[17]M. Garcia-Ratés, J.-C. de Hemptinne, J. B. Avalos, and C. Nieto-Draghi, "Molecular modeling of diffusion coefficient and ionic conductivity of CO_2 in aqueous ionic solutions," J. Phys. Chem. B **116**, 2787–2800 (2012).

[18]M. Javaheri, J. Abedi, and H. Hassanzadeh, "Linear stability analysis of double-diffusive convection in porous media, with application to geological storage of CO_2," Transp. Porous Med. **84**, 441–456 (2010).

[19]C. T. Tan and G. M. Homsy, "Stability of miscible displacements in porous media: Rectilinear flow," Phys. Fluids **29**, 3549–3556 (1986).

[20]D. A. S. Rees, A. Selim, and J. P. Ennis-King, "The instability of unsteady boundary layers in porous media," in *Emerging topics in heat and mass transfer in porous media*, theory and applications of transport in porous media No. 22, edited by P. Vadàsz (Springer Netherlands, 2008) pp. 85–110.

[21]P. M. J. Trevelyan, C. Almarcha, and A. De Wit, "Buoyancy-driven instabilities of miscible two-layer stratifications in porous media and Hele-Shaw cells," J. Fluid Mech. **670**, 38–65 (2011).

[22]S. Kalliadasis, J. Yang, and A. De Wit, "Fingering instabilities of exothermic reaction-diffusion fronts in porous media," Phys. Fluids **16**, 1395–1409 (2004).

[23]K. Ghesmat, H. Hassanzadeh, and J. Abedi, "The impact of geochemistry on convective mixing in a gravitationally unstable diffusive boundary layer in porous media: CO_2 storage in saline aquifers," J. Fluid Mech. **673**, 480–512 (2011).

[24]A. De Wit, "Fingering of chemical fronts in porous media," Phys. Rev. Lett. **87**, 054502 (2001).

[25]J. Ennis-King, I. Preston, and L. Paterson, "Onset of convection in anisotropic porous media subject to a rapid change in boundary conditions," Phys. Fluids **17**, 084107 (2005).

[26]X. Xu, S. Chen, and D. Zhang, "Convective stability analysis of the long-term storage of carbon dioxide in deep saline aquifers," Adv. Water Res. **29**, 397–407 (2006).

[27]M. Bestehorn and A. Firoozabadi, "Effect of fluctuations on the onset of density-driven convection in porous media," Phys. Fluids **24**, 114102 (2012).

[28]A. C. Slim and T. S. Ramakrishnan, "Onset and cessation of time-dependent, dissolution-driven convection in porous media," Phys. Fluids **22**, 124103 (2010).

[29]P. Cheng, M. Bestehorn, and A. Firoozabadi, "Effect of permeability anisotropy on buoyancy-driven flow for CO_2 sequestration in saline aquifers," Water Resour. Res. **48**, W09539 (2012).

[30]P. C. Myint and A. Firoozabadi, "Onset of buoyancy-driven convection in cartesian and cylindrical geometries," Phys. Fluids **25**, 044105 (2013).

[31]H. Hassanzadeh, M. Pooladi-Darvish, and D. W. Keith, "Stability of a fluid in a horizontal saturated porous layer: effect of non-linear concentration profile, initial, and boundary conditions," Transp. Porous Med. **65**, 193–211 (2006).

[32]A. Riaz, M. Hesse, H. A. Tchelepi, and F. M. Orr, "Onset of convection in a gravitationally unstable diffusive boundary layer in porous media," J. Fluid Mech. **548**, 87–111 (2006).

[33]C. Almarcha, P. M. J. Trevelyan, P. Grosfils, and A. De Wit, "Thermal effects on the diffusive layer convection instability of an exothermic acid-base reaction front," Phys. Rev. E **88**, 033009 (2013).

[34]J. Fernandez, P. Kurowski, P. Petitjeans, and E. Meiburg, "Density-driven unstable flows of miscible fluids in a Hele-Shaw cell," J. Fluid Mech. **451**, 239–260 (2002).

[35]M. T. Elenius and K. Johannsen, "On the time scales of nonlinear instability in miscible displacement porous media flow," Comput. Geosci. **16**, 901–911 (2012).

[36]W. M. Haynes, D. R. Lide, and T. J. Bruno, *CRC Handbook of Chemistry and Physics 2012-2013* (CRC Press, 2012).

[37]J. E. Garcià, "Density of aqueous solutions of CO_2," Tech. Rep. (Lawrence Berkeley National Laboratory, 2001).

[38]J. Martin, N. Rakotomalala, and D. Salin, "Gravitational instability of miscible fluids in a Hele-Shaw cell," Phys. Fluids **14**, 902–905 (2002).

[39]C. Almarcha, P. M. J. Trevelyan, L. A. Riolfo, A. Zalts, C. El Hasi, A. D'Onofrio, and A. De Wit, "Active role of a color indicator in buoyancy-driven instabilities of chemical fronts," J. Phys. Chem. Lett. **1**, 752–757 (2010).

[40]S. Kuster, L. A. Riolfo, A. Zalts, C. E. Hasi, C. Almarcha, P. M. J. Trevelyan, A. De Wit, and A. D'Onofrio, "Differential diffusion effects on buoyancy-driven instabilities of acid-base fronts: the case of a color indicator," Phys. Chem. Chem. Phys. **13**, 17295–17303 (2011).

[41]L. Lemaigre, M. A. Budroni, L. A. Riolfo, P. Grosfils, and A. De Wit, "Asymmetric Rayleigh-Taylor and double-diffusive fingers in reactive systems," Phys. Fluids **25**, 014103 (2013).

[42]M. Laliberté, "Model for calculating the viscosity of aqueous solutions," J. Chem. Eng. Data **52**, 321–335 (2007).

[43]W. Yan, S. Huang, and E. H. Stenby, "Measurement and modeling of CO_2 solubility in NaCl brine and CO_2 in saturated NaCl brine density," Int. J. Greenh. Gas Con. **5**, 1460–1477 (2011).

[44]M. Laliberté and W. E. Cooper, "Model for calculating the density of aqueous electrolyte solutions," J. Chem. Eng. Data **49**, 1141–1151 (2004).